Nuclear Engineering and Design 439 (2025) 114054

Contents lists available at ScienceDirect

Nuclear Engineering and Design

journal homepage: www.elsevier.com/locate/nucengdes

Multiphysics modeling approach for the analysis of noble metals deposition in the Molten Salt Fast Reactor

Nicolò Iaselli [a], Antonio Cammi [a,b], Stefano Lorenzi [a,*]

[a] Politecnico di Milano, Department of Energy, 34, Via La Masa, 20156 Milan, Italy
[b] Khalifa University, Emirates Nuclear Technology Center (ENTC), Department of Mechanical and Nuclear Engineering, 127788 Abu Dhabi, United Arab Emirates

ARTICLE INFO

Dataset link: http://doi.org/10.5281/zenodo.14017301

Keywords:
Molten Salt Fast Reactor (MSFR)
Multiphysics
OpenFOAM
Particle deposition
Noble metals

ABSTRACT

Noble metals exhibit very low solubility in fluorine salts, leading to accumulation on reactor surfaces, which negatively impacts performance and safety. In this work, a new modeling capability of the OpenFOAM multiphysics solver, developed at Politecnico di Milano is proposed to analyze the deposition of noble metal fission products in the Molten Salt Fast Reactor (MSFR). To model the particle migration towards reactor walls, a tailored particle transport model and custom boundary condition were implemented. Verification against an analytical solution confirmed accuracy, followed by a sensitivity analysis on mesh refinement, which demonstrated strong dependence on wall-adjacent cell size. Simulating the reactor in full geometry and accounting for all nuclides in the salt demands high-performance computational resources, even for steady state conditions. To reduce computational effort, the deposition velocity (or mass transfer coefficient) obtained from a highly refined mesh was applied to coarser meshes using the tailored boundary conditions. This approach, combined with a single pseudo-nuclide representing the noble metals family, significantly reduces computational demand. Different mesh types were tested for steady-state reactor core simulations, showing that the deposition velocity-based strategy provides satisfactory results for the quantities of interest. Preliminary results are also presented for decay heat generated by radioactive particle deposits. The developed capability to describe noble metal behavior advances the multiphysics solver and contributes to the MSFR's design optimization.

1. Introduction

Molten Salt Reactors have been selected by the Generation IV International Forum as one of the six promising nuclear technologies for commercial power production. In particular, the fluoride-based Molten Salt Fast Reactor has been chosen as the reference design within the SAMOSAFER European project. In particular, this is a thorium-breeding reactor, employing a homogeneous mixture of LiF (77.5 mol%), $^{232}ThF_4$ (20 mol%) and $^{233}UF_4$ (2.5 mol%), which acts simultaneously as fissile, fertile and coolant. This peculiar configuration allows for many significant improvements over conventional reactors, both from the safety and resources utilization point of view. On the other hand, the presence of a circulating fuel poses several technical challenges, which require custom-made simulation tools to be overcome (Aufiero et al., 2014; Fiorina et al., 2014).

In MSFRs, and generally in circulating-fuel reactors, fission products (FPs) are not retained within the primary and secondary barriers (i.e., the fuel pellet itself and the cladding). Instead, they are carried away by the salt flow immediately after being produced by fission events. This requires accounting for thermochemical interactions between the salt, FPs, and wall materials (Scuro et al., 2024; Stempniewicz and Roelofs, 2021), while also modeling the deposition of solid FPs, which will be the main focus of this paper. Among all the possible FPs species, noble metals exhibit the lowest affinity for fluorine, hence having the tendency to precipitate, agglomerate, and eventually deposit on reactor surfaces. Noble metals, as observed repeatedly during the Molten Salt Reactor Experiment (Kedl, 1972), tend to accumulate at specific locations. The most significant are the Primary Heat Exchanger (PHX), due to its large surface area and surface-to-volume ratio, and the off-gas system, driven by bubbling and gas impinging on the salt near free surfaces. Critical implications of this phenomenon include detriment to heat transfer performance, partial flow blockage, and eventually damage to structural materials. These effects can be somewhat concerning in steady-state conditions, but are particularly relevant during accident scenarios; for example, the additional heat flux produced by particle decay during a core draining. Furthermore, these surface deposits present serious radiological risks

* Corresponding author.
E-mail address: stefano.lorenzi@polimi.it (S. Lorenzi).

https://doi.org/10.1016/j.nucengdes.2025.114054
Received 19 December 2024; Received in revised form 21 February 2025; Accepted 3 April 2025
Available online 3 May 2025

during inspection and maintenance operations, necessitating careful monitoring and management to ensure the safety of personnel and the operational integrity of the reactor. Considering the specific thermo-chemical environment of the MSFR, a small group of elements known as Five Metals (5Ms) – namely Molybdenum, Technetium, Ruthenium, Rhodium, and Palladium – is extremely insoluble in fluorides (Benes and Konings, 2012), and will be the focus of this work. Although recent studies on FP transport in MSFRs are limited, understanding their distribution in the reactor core is crucial for reactor design, especially concerning removal/reprocessing (Delpech et al., 2009) and helium bubbling system (Cervi et al., 2019). Recent work has focused on modeling Xenon transport behavior in MSRs (Price et al., 2020). Concerning metallic FPs, their behavior has been analyzed using a multiphysics system code applied to the Molten Salt Reactor Experiment (Walker and Ji, 2021).

The aim of this work is to equip state-of-the-art MSFR multiphysics codes with new features to model particle transport, while at the same time developing a strategy to abate computational intensity of complex simulations. Following previous studies on the subject (Di Ronco et al., 2022), a single-phase fully Eulerian approach is chosen. This represents a commonly employed and versatile tool for particle transport modeling in a number of different scenarios, from the nuclear field (Gladinez et al., 2019; Marino et al., 2020) to broader applications (Krause et al., 2013; Frederix et al., 2017). The Computational Fluid Dynamics (CFD) library OpenFOAM (Jasak, 2009) has been chosen to leverage previous efforts on the topic and for the flexibility of the widely-used open-source platform.

A set of implementations to the reference multiphysics model and related approach will be presented. First, a tailored boundary condition is introduced to properly solve the particle transport problem. Based on the deposition velocity, it represents the local behavior of 5Ms particles in proximity to reactor surfaces. The upgraded model is then verified against the analytical solution for a deposition problem in a two-dimensional laminar flow (Di Ronco et al., 2021). Afterward, the model is used to perform a mesh sensitivity analysis on a simplified two-dimensional wedge geometry; the influence of wall refinement is discussed from the physical and computational point of view. The natural step forward is solving particle transport in a more realistic MSFR environment, which unfortunately comes at the cost of increased processing demand due to the geometrical complexity and multitude of 5Ms nuclides present. To cope with this second issue, a Pseudo-nuclide is introduced, embodying the characteristic behavior of the family as a whole. The reduction of computational expense, on the other hand, is achieved through the use of the aforementioned boundary condition, which allows the exploitation of accurate results from a highly-refined mesh to model particles in a much coarser one. This strategy can be applied to steady state simulations – and possibly selected transients – in order to reduce computational requirements and enable more complex analyses of the MSFR core. Finally, some preliminary results are presented concerning the heat flux generated at the walls from the radioactive decay of deposited 5Ms particles.

2. Multiphysics model

Different iterations of the OpenFOAM multiphysics model have been developed at the Politecnico di Milano starting with coupled neutronics and thermal-hydraulics (Aufiero et al., 2014; Fiorina et al., 2014), moving on to helium bubbling (Caruggi, 2021), and transport of solid fission products (Di Ronco et al., 2021). The following work is based on the latest version of the solver branch dedicated to modeling particle transport (Di Ronco et al., 2022).

Most of the equations already included in the solver are here omitted since they have not been substantially modified, and are of marginal relevance to the work that follows. However, in order to provide a clear context of the implementations, it is important to describe briefly the main elements of the iteration scheme, as shown in Fig. 1. Starting from the top, the first block is dedicated to solving the thermal-hydraulics problem through the standard SIMPLE algorithm for pressure–velocity coupling (Patankar and Spalding, 1972), similar to the *simpleFoam* solver distributed with the standard OpenFOAM library. In particular, this subroutine solves incompressible, Reynolds-Averaged Navier–Stokes (RANS) equations with Boussinesq buoyancy assumption and standard eddy viscosity-based closure models, such as the well-known k-ϵ model (Launder and Spalding, 1974). The outputs of this step – namely velocity, temperature and pressure fields – are sequentially used to perform iterations within the neutronics subroutine. The solver employs a multi-group diffusion model for neutron flux calculations (Hébert, 2010), which balances fidelity and computational effort effectively (Aufiero et al., 2014; Fiorina et al., 2016). First, group constants are updated to account for Doppler and density effects due to local changes in temperature; then, group-wise neutron fluxes are solved, followed by neutron and decay heat precursors. Thanks to these quantities, it is possible to calculate the heat released by all the implemented neutron reactions at each point of the reactor core—i.e., update the power source. It is important to note that, given the circulating nature of the fuel, precursors are transported by the salt flow. At this point, the segregated nature of the outer iteration scheme is evident looking at how the two subroutines are coupled; in turns, one is kept frozen while used as input for the other one until some convergence criteria are met.

As a final subroutine, the model for the transport of fission products is implemented in a one-way coupling fashion (Di Ronco et al., 2021). This will be the focus of the present work. Each fission product species is modeled as a concentration field subject to advection, dispersion (i.e., diffusion) and decay:

$$\frac{\partial c}{\partial t} + \nabla \cdot (\mathbf{u}c) = \nabla \cdot \left(D_{eff} \nabla c \right) - \lambda c + S \tag{1}$$

where c is the volumetric concentration of a certain species, D_{eff} is the RANS formulation – i.e., the sum of a laminar and turbulent contribution – of particle diffusivity, $\mathbf{u}$ is the velocity vector of the carrier, and λ and S are the decay constant and source rate, respectively, of said species. Assuming that chemical interactions and formation of new phases can be neglected in favor of a more streamlined integration of the proposed features, the source term can be reduced to the sole generation from fission:

$$S = y_f \sum_g \Sigma_{f,g} \varphi_g \tag{2}$$

where y_f is the fission yield coefficient, and the terms inside the summation represent the group-wise fission rate.

The single-phase Eulerian approach followed is expected to yield comparable results with respect to other strategies (e.g., Eulerian-Eulerian multiphase or Eulerian-Lagrangian), with the added benefit of a much simpler modeling framework. This claim is valid if two main conditions are met. First, whether Fick's diffusion law is applicable, meaning that inertial effects can be neglected due to sufficiently small particle size (Liu and Agarwal, 1974). Unfortunately, very little information is available about particle size distribution in the MSFR. The most relevant evidence in this context comes from analysis on deposited noble metals conducted at MSRE (Compere et al., 1975), where colloidal suspensions – with diameters ranging from nm to μm – were hypothesized. The second condition is that particle concentration is low enough to neglect interactions between the particles and the fluid, or among particles themselves. These hypotheses are assumed to hold throughout the presented work to avoid the need of implementing a dedicated framework for particle interaction and clustering. This choice allows minimizing the overall complexity to introduce a more straightforward approach for the modeling of noble metals deposition.

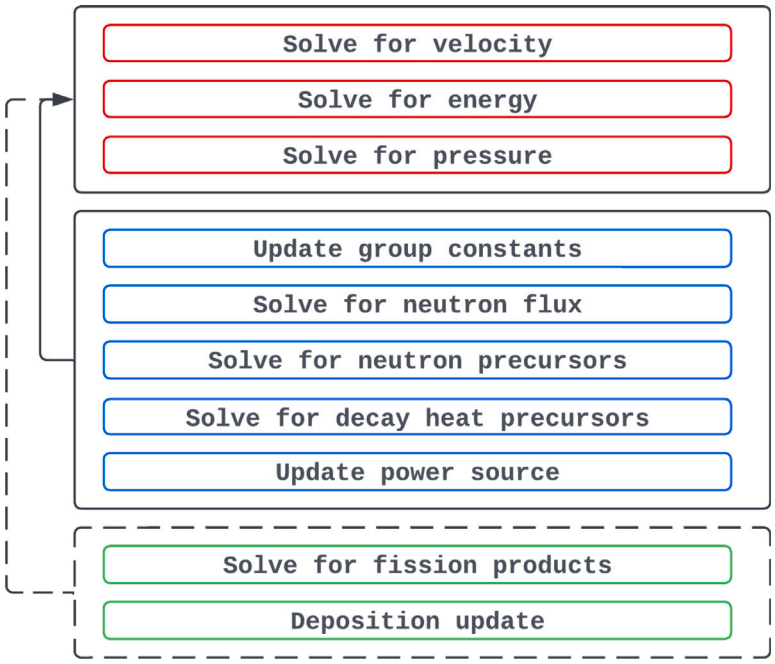

Fig. 1. Outer iteration scheme featured in the OpenFOAM multiphysics solver.

3. Noble metals deposition modeling

As anticipated, noble metals show extremely low solubility in the MSFR salt, with a metal fluorides to metal ions ratio in the order of 10^{-10} or lower (Benes and Konings, 2012) (although greatly dependent on the redox potential of the salt). This indicates that the particles will inevitably precipitate and quickly build up on the reactor surfaces. With time, this could lead to a serious degradation of heat extraction from the primary loop, and to an additional radioactive source to be taken into account for reactor transients, or during inspection and maintenance operations. The modeling of the 5Ms group is implemented starting from the generic fission products transport model presented in Section 2. The two essential additions are the custom boundary condition – linking the particle concentration field to the deposition phenomenon – and the representative nuclide for 5Ms particle species, or 'Pseudo-nuclide', to alleviate computational effort.

3.1. Deposition boundary condition

The transport equation for noble metals requires a proper boundary condition in order to be solved – and return physically sound results – which prompted the idea of introducing one that is tailored to the specific case. As investigated in numerous works (Brenner, 1961; Ruckenstein and Prieve, 1973; Prieve and Ruckenstein, 1976), the deposition phenomena can be seen as driven by the so-called reaction potential energy ϕ. This quantity, as shown in Fig. 2, is negligible in the bulk of the fluid, then it peaks very close to the wall before abruptly going to zero at the surface. In fact, it embodies the likelihood for a particle to deposit on reactor walls, which is relevant only at distances comparable to the characteristic length (δ_ϕ) of the deposition phenomenon. This behavior suggests the possibility to decouple the particle transport domain in an advection-driven region – i.e., the bulk flow – and a thin boundary region characterized by a purely diffusional regime—i.e., the immediate surroundings of the wall. As a consequence, the entire wall region can be condensed into a first-order reaction boundary condition to be applied to the bulk particle concentration. The one-dimensional formulation (Ruckenstein and Prieve, 1973; Prieve and Ruckenstein, 1976) is the following:

$$D^{\infty}_{eff}\frac{\partial c}{\partial y} = \gamma c, \qquad y = 0 \tag{3}$$

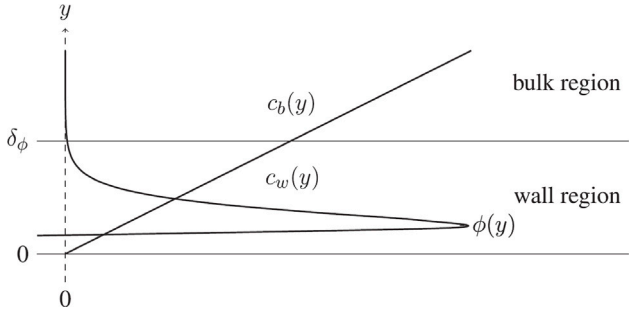

Fig. 2. Decoupling of the advection and diffusion-driven regions. On the y-axis, the distance from the wall surface. The x-axis indicates reaction potential energy.

where D^{∞}_{eff} is the diffusion coefficient outside the deposition boundary layer and γ is the so-called deposition velocity. This quantity, having the dimensions of a proper velocity, describes the behavior of particles depositing on various surfaces and can be seen as the mass transfer coefficient for said particles. The exact formulation of γ is here omitted; however, it is important to note that it depends on a multitude of parameters (e.g., the reaction potential and boundary layer thickness) that are not known a priori for conditions typical of the MSFR core. Nevertheless, (3) can be rewritten in the three-dimensional form, with a notation that is more suited for the implementation in the multiphysics OpenFOAM solver:

$$-D^{\infty}_{eff}\nabla c \cdot \mathbf{n} = \gamma c \tag{4}$$

where $\nabla c \cdot \mathbf{n}$ is the wall-normal gradient of particle concentration.

Considering the critical role of the deposition velocity for the development of this work, a few key points must be addressed. Most importantly, as shown in Fig. 2, the calculation of this quantity requires fully resolving the particle concentration field. This arises from the deposition phenomena unfolding within a very thin boundary layer, which necessitates a certain level of mesh refinement to achieve satisfactory accuracy in the results, a topic that will be revisited throughout. The required refinement is ultimately defined by the wall-adjacent cell size, which spatially represents the diffusion-driven boundary layer,

analogous to the well-known use of wall functions in conventional CFD modeling. It is also important to note that the requirements for the deposition phenomenon are expected to be very different from those for other physics involved in the simulation of the MSFR. In particular, the solution of multi-group diffusion is weakly dependent on average cell size and refinement at the walls; the main benefit of a fine mesh would be the spatial resolution of the output field, with marginal impact on the overall accuracy of the results. For what concerns RANS-based fluid dynamics, since only the average turbulence is resolved – rather than the full turbulence spectrum – there is very little return in refining the mesh at the walls past the size required to properly implement wall functions. In principle, it is possible to modify the multiphysics solver to tackle different physics on different meshes, thanks to the use of field mapping algorithms that operate between iteration steps (Chourdakis et al., 2023). While effective in reducing computational intensity, this strategy would still require a highly refined mesh to resolve the strong gradients involved in particle deposition. For this reason, it was decided to follow a more straightforward OpenFOAM code development to focus on the implementation of 5Ms transport and deposition modeling, leaving the realization of such algorithms to future endeavors. As a final consideration, since it is currently impossible – due to the absence of suitable experimental results in this context – to infer a certain value of deposition velocity, the boundary condition cannot be used immediately without the risk of heavily altering the fidelity of the model.

The proposed solution to these issues is to first postulate a conventional, yet reasonable boundary condition that does not require some a priori quantitative and localized information on the deposition phenomenon. The most suitable assumption is to consider perfectly absorbing walls, which implies particle concentration approaching zero (or infinite reaction potential) towards the surface. Thanks to this approach, it is possible to solve the noble metals transport equation in steady state with physically sound results. It should also be noted that, given the very slow dynamic of deposition, the calculated field can be used as an initial condition for future transient simulations. By doing this, it would be possible to assess the impact of the 5Ms decay heat during safety critical scenarios.

However, as mentioned previously, the thinness of the deposition boundary layer requires fully resolving strong wall-normal gradients, leading to increasingly larger computational effort. To alleviate this problem, the strategy is to first perform a reference simulation on a highly refined mesh, from which the deposition velocity is calculated as follows:

$$\gamma = -D\frac{\nabla c \cdot \mathbf{n}}{c} \tag{5}$$

The deposition velocity is then used as input for the boundary condition, as in Eq. (4), for much coarser meshes. In Section 5 this strategy will be applied to the simulation of the MSFR geometry, with satisfactory results.

3.2. Deposition and decay heat fields calculation

The proposed boundary condition (4) can be seen as the implementation of a sink term that removes particles from the bulk concentration and, consequently, a source term acting on the deposition field. Thus, it is possible to introduce a straightforward balance equation to model the evolution in time of the concentration of deposited particles d—i.e., the number of particles per unitary surface area that are attached to the wall. Such balance equation takes the following form:

$$\frac{\partial d}{\partial t} = -(\lambda + \xi)d + \gamma c \tag{6}$$

where λ, ξ, γ are the decay constant, desorption rate and deposition velocity of the particle species under analysis. It is here stated that the value for ξ is kept at zero for all applications of the multiphysics presented in this work. This is a compelled choice – which also happens to be a conservative one – due to the lack of suitable experimental values to be employed in the desorption model. Similarly to the transport equation for the bulk flow, this balance should be implemented for a large number of species, each with additional sink and source terms to account for the complex system of decay chains. However, explicitly tracking all the possible cross-contributions from hundreds of nuclides featuring greatly diverse half-lives, would require exceptional computational resources. The choice was to neglect these contributions and focus on the equilibrium state where the particle concentration is simply due to the balance between production, deposition and radioactive decay of the selected species. Moreover, the increasing thickness of the deposited layer is not modeled, since it would require the use of a deforming mesh and Conjugate Heat Transfer solvers to simulate coupled convective and conductive phenomena. Instead, the choice was to prioritize the concentration of radioactive particles present in the layer itself, which is particularly useful to assess the impact of 5Ms radioactive decay on reactor walls.

The decay heat flux (in W/m^2) is obtained through the following equation, which is solved immediately after the deposition balance in (6), and thus does not require further numerical iterations:

$$q'' = dQ_d \tag{7}$$

where Q_d (W) is the calculated decay heat per unstable deposited particle, as discussed in the following section.

3.3. The Pseudo-nuclide approach

As mentioned earlier, in order to obtain a complete picture of the 5Ms particle behavior, both the transport and deposition equations – including cross-contributions from all the possible decay chains – should be solved for each of the nuclides of the family. This would evidently require a considerable amount of computational resources to reach acceptable levels of accuracy within the solving algorithm. To avoid this problem, a Pseudo-nuclide approach is used.

The different isotopes belonging to the 5Ms family show essentially identical chemical-physical properties—mainly very low solubility in the salt, and strong tendency to form alloys with other members of the group. From the nuclear point of view the radionuclides present a rather diverse behavior, both in terms of decay constant and energy released from decay. The proposed method aims at condensing all this information into a single Pseudo-nuclide that is able to describe, as an approximation, the main features of the noble metals family.

The first step consists in running a simplified SERPENT 2 Monte Carlo simulation of the MSFR at steady state with no fresh salt feeding or reprocessing. This simulation has been run in previous efforts (Bittesnich, 2022), so that the individual effective fission yields could be extracted for all the nuclides included in the simulation as follows:

$$y_{eff,i} = \frac{N_i}{BU} \tag{8}$$

where N_i is the atomic concentration of a certain species and BU is the fuel burnup. By calculating yields in this way, it is implicitly assumed that the equilibrium condition is representative of the MSFR environment in general. Although such reasoning would imply neglecting the effects of decay chains, it is also true that at steady state the contribution of radionuclides that reached equilibrium is dominant. The particle source term presented in (2) can be rewritten as:

$$S = y_{tot}\sum_g \Sigma_{f,g}\varphi_g \tag{9}$$

where y_{tot} is the overall fission yield of all the nuclides that belong to the 5Ms family.

The resulting Pseudo-nuclide is then assumed to be a homogeneous mixture of active particles, individually weighted on their respective effective fission yield. The effective decay constant is derived starting from the calculation of the activity of such a hypothetical mixture:

$$A_{mix} = \sum_{i=1}^{n}\lambda_i N_i = \lambda_{eff} N_{tot} \tag{10}$$

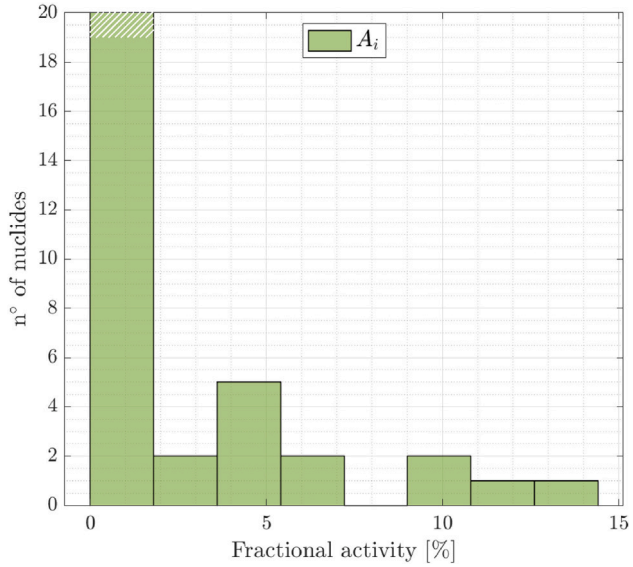

Fig. 3. Contributions to the activity of the Pseudo-nuclide. The shaded area represents an out-of-bounds value.

Table 1
Physical and nuclear properties of the 5Ms and metals Pseudo-nuclides.

Quantity	5Ms	Metals
ρ (g/cm^3)	10.98	6.79
d_p (nm)	0.370	0.437
y_{tot} (-)	0.295	1.248
λ_{eff} (s^{-1})	6.614×10^{-9}	2.336×10^{-8}
Q_{eff} (W/part.)	2.146×10^{-21}	9.335×10^{-21}

$$\lambda_{eff} = \frac{1}{y_{tot}} \sum_{i=1}^{n} \lambda_i y_i \tag{11}$$

As a consequence, a single instance of both the transport and deposition equations is solved employing as sink the effective decay terms, $\lambda_{eff} c$ and $\lambda_{eff} d$ respectively. In Fig. 3 are shown the individual contributions to the overall activity, from which it is evident that almost 90% of the radioactivity is due to a few nuclides only—a dozen out of almost two hundred in total.

The second key quantity is the effective decay heat released by the layer that has been depositing onto the reactor walls, which is computed following the same homogeneous mixture approach:

$$Q_{mix} = \sum_{i=1}^{n} \left(\lambda_i E_{d,i}\right) N_i = Q_{eff} N_{tot} \tag{12}$$

$$Q_{eff} = \frac{1}{y_{tot}} \sum_{i=1}^{n} \left(\lambda_i E_{d,i}\right) y_i \tag{13}$$

where $E_{d,i}$ is the energy release in the decay of the ith nuclide. It is important to note that, given the Pseudo-nuclide approach followed, the quantity Q_{eff} must then be multiplied by concentration of deposited particles d to obtain the heat flux delivered to the reactor walls.

Finally, to recap the features of the Pseudo-nuclide derived for 5Ms and to compare them with the equivalent entities for all the other metals, Table 1 summarizes the most relevant physical and nuclear properties.

4. Model verification and sensitivity analysis

4.1. Model verification

In order to assess the proper functioning of the multiphysics code implementation, a verification against analytical solutions is performed.

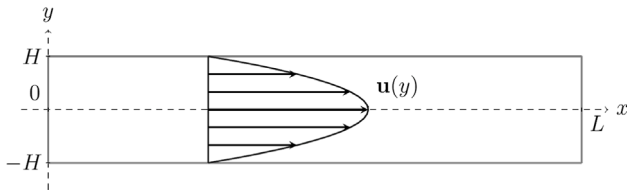

Fig. 4. Simulation domain employed in the simplified verification case.

Table 2
Key properties employed in the verification case.

Parameter	Value	Units
Center-line velocity	0.5	m s^{-1}
Kinematic viscosity	5×10^{-5}	m^2 s^{-1}
Particle mass diffusivity	5×10^{-5}	m^2 s^{-1}
Decay constant	2×10^{-3}	m^2 s^{-1}

The aim is ensuring that particles modeling – meaning bulk transport and deposition boundary condition – is physically sound and delivers the expected results. Inconveniently, the complexity of the MSFR geometry and environment would lead to a challenging one-to-one verification process. This requires the use of a simplified domain to leverage the work of Di Ronco et al. (2021), which proposes an analytical solution for a pipe flow with distributed particle source, linear decay and deposition (also known as an extended Graetz problem). However, the verification strictly assumes steady-state conditions, precluding time-dependent verification. Considering the characteristic timescales of particle deposition and the intended applications of the code, such an analysis was not deemed essential for evaluating the suitability of the code to produce meaningful results. Nevertheless, modeling deposition as a function of time remains significant in the MSFR field, and represents a relevant area for future investigation. Due to the complexity of the analytical solution and its limited additional insight, the results are directly compared in the following.

The geometry of the verification case consists of a horizontal channel where salt flows from left to right with a perfectly parabolic velocity profile, as shown in Fig. 4. In OpenFOAM, inlet and outlet velocity boundary conditions are set to null gradient, while the outlet pressure is set to zero for increased solver stability. A cosine-shaped particle source term is introduced along the axis of the channel, which is a justified assumption for neutron flux-related quantities in nuclear reactors.

The simulation is performed using properties compatible with a fully developed laminar flow, as summarized in Table 2. Tight tolerances are set for the iteration variables (from 10^{-6} to 10^{-9}) in order to achieve the high accuracy required for the evaluation against the analytical solution. The results obtained at the end of the simulation, in terms of normalized particle concentration at different channel longitudinal coordinates, are in excellent agreement with the theory, as clearly shown in Fig. 5.

4.2. Preliminary sensitivity analysis

As already mentioned, a clear correlation is expected, due to the strong gradients involved, between the deposition quantities and the refinement level of the mesh used to simulate in OpenFOAM. In order to have a quantitative understanding of this issue, a preliminary sensitivity analysis is performed on the EVOL reactor (see Fig. 6), which has been used as reference in previous endeavors concerning the European MSFR development (Brovchenko and Merle, 2013). The domain is a simplified two-dimensional wedge of the primary loop, featuring sharp edges that easily enable highly regular meshing. Fuel salt momentum source – in a clockwise fashion – and heat sink are taken into account through the use of OpenFOAM cell zone, respectively called Pump and HX in Fig. 6.

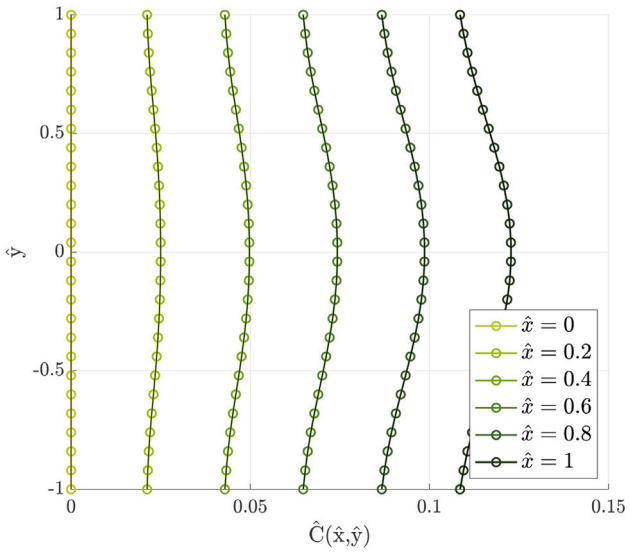

Fig. 5. Comparison of normalized concentration profiles $\hat{C}(\hat{x},\hat{y})$ at given normalized lengths $\hat{x}$, obtained with the proposed multiphysics model (∘) and the respective analytical value (–).

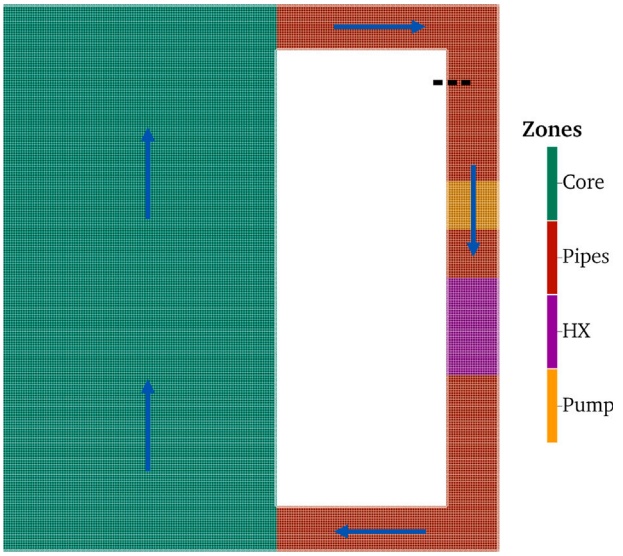

Fig. 6. Reactor zones implemented in the Evol reactor simulation domain. The dashed line indicates the sampling location.

The objective is to analyze dependency of the particle concentration and deposition fields on the wall-adjacent cell size, assuming perfectly absorbing walls for consistency. The deposition field is inspected at a prescribed, yet arbitrary, location upwind to the foreseen insoluble FPs removal system, as shown in Fig. 6. The particle concentration field, as a consequence, is sampled in the region neighboring the chosen point on the reactor surface. As it will be further discussed in Section 6, the local deposition field is greatly influenced by geometry and salt flow patterns, which means that a single cell-wise value can be somewhat misleading when comparing different simulation domains and scenarios. Therefore, the results of the sensitivity analysis should not be seen as a comprehensive description of particle behavior in the reactor core and cooling loop, but rather as indicative of the general characteristics of the deposition phenomenon.

All cases are run using the parameters summarized in Table 3, and with comparable solver tolerances. A total of 25 simulations are performed with wall-adjacent cell size – hereby denoted by δ – ranging

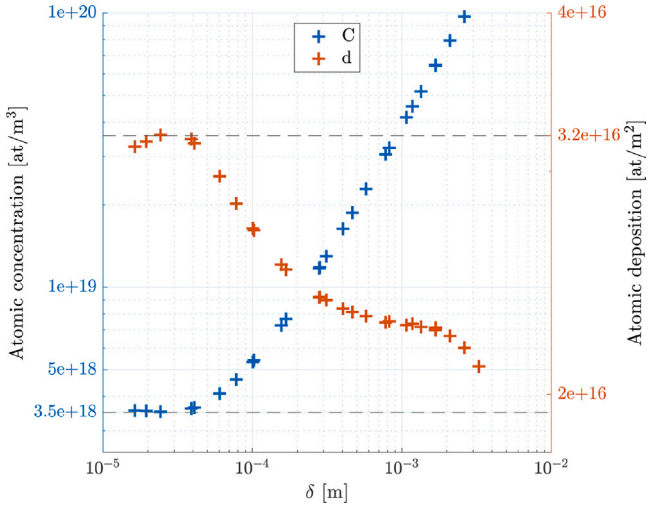

Fig. 7. Results of the sensitivity analysis performed using the proposed multiphysics model for the EVOL reactor case.

from 3 mm down to 15 μm. As can be seen in Fig. 7, the imposed δ follows a logarithmic spanning, albeit not rigorously so due to the refinement algorithm employed. It is also important to note that the mentioned cell sizes refer to the cell side normal to the wall, while the other cell dimension is occasionally adjusted to maintain a mesh aspect ratio compatible with the numerical solvers employed. Nevertheless, it is evident from the plot that both variables converge once a sufficiently small wall-adjacent cell size – in the order of a few tens of microns – is reached. This value, even if extracted from a simplified scenario, can be considered a valuable reference for the simulation of the deposition phenomenon in the MSFR environment. Moreover, the particle concentration in the bulk is shown to be inversely proportional to the proximal deposition. Such behavior is physically sound, considering that a locally stronger deposition regime implies a lower number of particles dispersed in the fuel salt at equilibrium. The total number of deposited particles, on the other hand, remains roughly constant at around 3×10^{16}, regardless of the refinement profile employed.

5. MSFR simulation case

5.1. Geometry and simulation setup

To further investigate the characteristics of the deposition phenomenon in the framework of the SAMOSAFER project, a more refined reactor geometry has been adopted for the steady-state analysis. This geometry is represented by a 1/16th three-dimensional section of the MSFR primary circuit, hence the smallest symmetrical unit that includes one of the 16 heat exchangers foreseen by the current design. Simplified regions are introduced to establish appropriate boundary conditions and offer a basic depiction of the primary components, as shown in Fig. 8.

Firstly, the core region features symmetry conditions on the two opposed cutting planes, as well as generic wall boundary conditions for the blanket (i.e., the curved surface enclosing the reactor core) and for the lower and upper reflectors. The cooling circuit is modeled employing wall boundary conditions throughout the whole structure, while the pump and heat exchanger are represented by regions of volumetric momentum source and heat sink, respectively. This approach comes with a rather significant approximation in comparison to the foreseen complex structure of the components, but serve the important purpose of defining the dominant flow behavior in the reactor core. It is important to note that no particle filtering and extraction system is implemented in the MSFR simulation domain, possibly leading to very

Table 3
Key simulation parameters employed in the EVOL reactor case.

Parameter	Value	Units
Turbulence model	k-ϵ	–
Density	4.307×10^{3}	kg m^{-3}
Kinematic viscosity	5.89×10^{-6}	m^2 s^{-1}
Specific heat capacity	1.594×10^{3}	J kg^{-1} K^{-1}
Thermal expansion coefficient	1.912×10^{-4}	K^{-1}
Reference temperature	973	K
Prandtl number	23.78	–
Turbulent Prandtl number	0.85	–
Schmidt number	calculated	–
Turbulent Schmidt number	0.85	–
Heat removal coefficient	2.5×10^{6}	W m^{-2} K^{-1}
Heat sink temperature	900	K

Table 4
Key simulation parameters employed in the MSFR case.

Parameter	Value	Units
Turbulence model	k-ϵ	–
Density	4.307×10^{3}	kg m^{-3}
Kinematic viscosity	5.89×10^{-6}	m^2 s^{-1}
Specific heat capacity	1.594×10^{3}	J kg^{-1} K^{-1}
Thermal expansion coefficient	1.912×10^{-4}	K^{-1}
Reference temperature	973	K
Prandtl number	23.78	–
Turbulent Prandtl number	0.85	–
Schmidt number	Calculated	–
Turbulent Schmidt number	0.85	–
Thermal power	187.5	MW
Heat removal coefficient	2.5×10^{7}	W m^{-2} K^{-1}
Heat sink temperature	900	K
Pump mass flow rate	1187.5	Kg s^{-1}

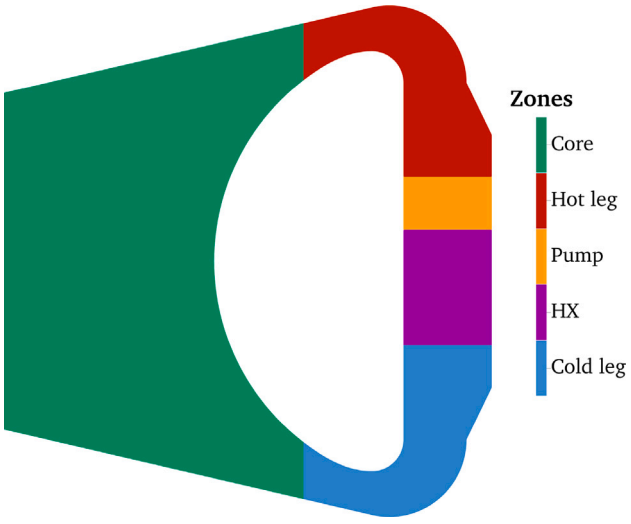

Fig. 8. Reactor zones implemented in the MSFR simulation domain.

large deposition rates. The effect of such a component on the quantities of interest is tangential to the scope of this work, and its analysis is left to future endeavors on the subject. The key settings and parameters employed for all MSFR simulation cases are similar to the ones used earlier for the EVOL reactor core, which could already be considered close to a realistic case scenario and are displayed in Table 4.

To help understand the environment in which the deposition phenomenon takes place, it is important to make some considerations on the most relevant MSFR core quantities (shown in Fig. 9). Starting with the salt velocity field, the flow pattern due to the clockwise motion imparted by the pump can be seen, in addition to the local turbulent features throughout the cooling circuit.

With respect to temperature, the effect of the ideal heat exchanger is clearly visible, since the entirety of the primary flow is cooled down by the volumetric heat sink so that it re-enters the core at exactly 900 K. The pressure field is dominated by the hydrostatic term, as can be seen by the nearly horizontal isobaric lines, and it is only locally impacted by the kinematic and dynamic contributions. Most importantly, it is lower than 2 bars gauge everywhere, in accordance with the low level of pressurization expected for the MSFR primary circuit design. Lastly, the fission rate field, which represents the source term for noble metal particles, follows closely the functional shape of the neutron flux in a finite cylinder. Noble metals are therefore mainly produced within the innermost region, are then spread around the primary fuel loop by advection and dispersion, and eventually undergo decay and deposition.

5.2. Mesh refinement

The preliminary sensitivity analysis discussed in Section 4.2 showed the correlation between deposition quantities and the level of mesh refinement, with a particularly strong effect that can alter the fidelity of a specific simulation. A similar meshing approach is followed in this case, with consecutive divisions of the wall-adjacent cell layer leading to the desired refinement profile, as shown in Fig. 10. However, unlike the simplified geometry of the EVOL reactor, the MSFR simulation domain features curved surfaces with different radii and sharp edges where the pump and the primary heat exchanger are located. Consequently, the quality of the mesh – and thus numerical solvers stability – has been notably sensitive to the chosen algorithm and its settings.

In light of this, six different mesh types are generated to perform simulations of the MSFR core. As can be seen from table Table 5, wall-adjacent cell size δ is decreased from a fully coarse value (i.e., no refinement at all) down to 300 μm. Although a detailed description of the meshing approach is beyond the scope of this work, it should be noted that a more extended refinement sweep was not achievable due to the rapid increase in cell count needed to maintain manageable aspect ratios (roughly below 50). Nevertheless, the sensitivity analysis

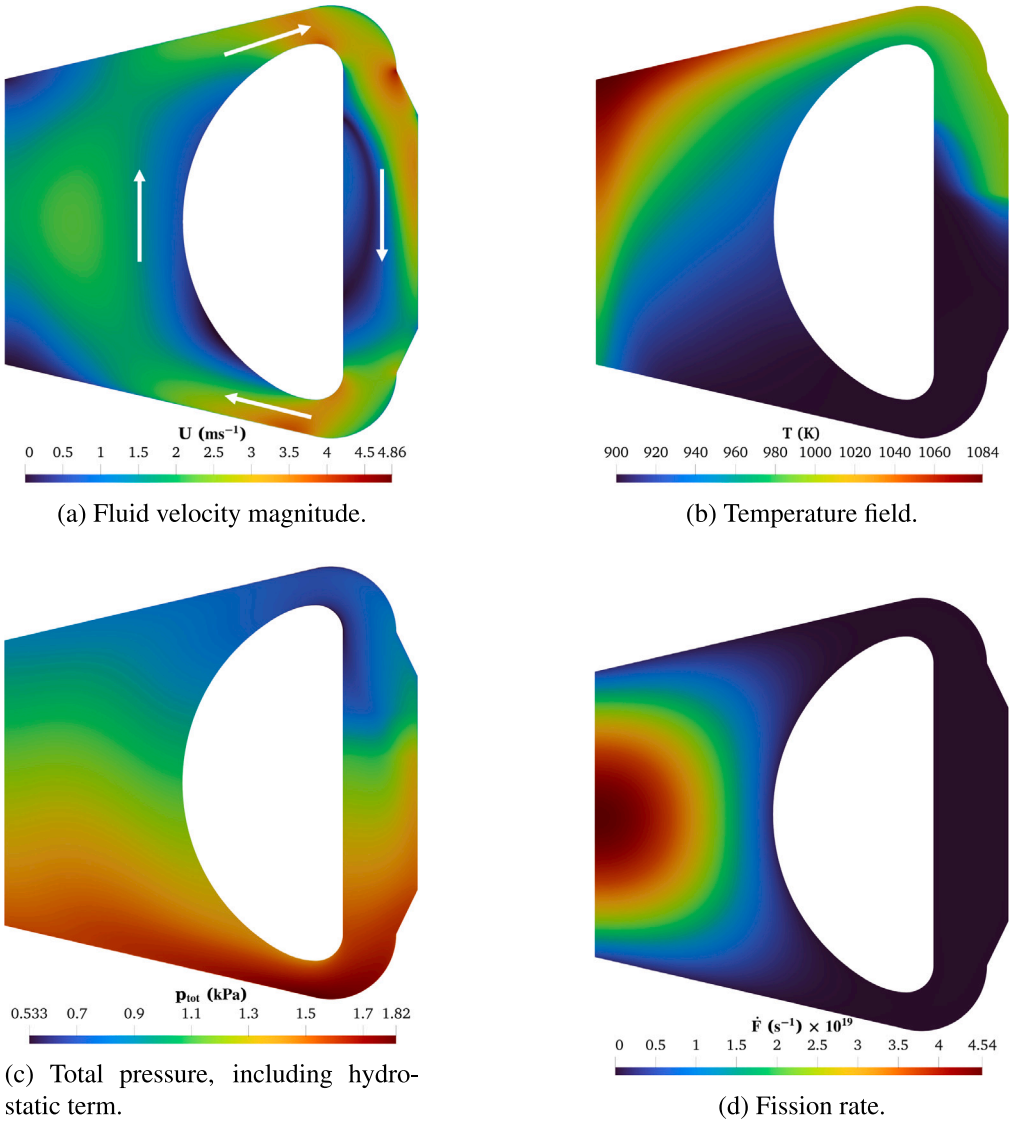

(a) Fluid velocity magnitude.

(b) Temperature field.

(c) Total pressure, including hydrostatic term.

(d) Fission rate.

Fig. 9. Key calculated quantity fields in the MSFR case.

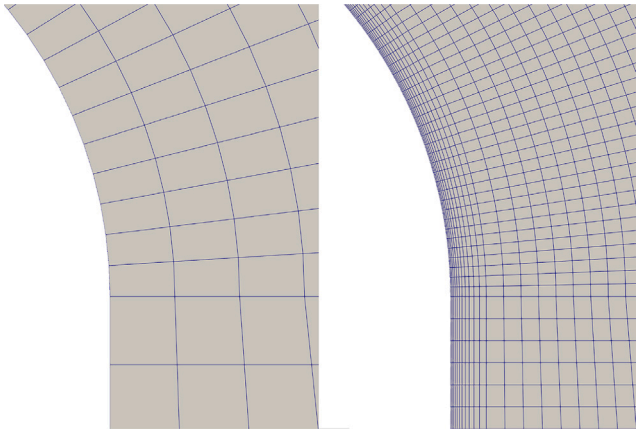

Fig. 10. Comparison between MSFR mesh type 1 (most coarse) and 6 (most refined). Lower hot leg region.

discussed in Section 4.2 can represent a good indicator of the proximity to convergence.

6. Results and discussion

6.1. Perfectly absorbing walls

As mentioned previously, no a priori value for the deposition velocity is available for the peculiar environment of the MSFR core. In light of this, the case is run employing the 6 mesh types and assuming perfectly absorbing walls, which represent the simplest, yet physically sound boundary condition for the deposition phenomenon. After inspecting the results, it emerged that particle concentration is only slightly affected in its macroscopic distribution by the features of the mesh. This behavior is reasonable because, even considering the reduction in base cell size collateral to the refinement, all mesh types are likely fine enough to resolve bulk particle transport. On the other hand, the values of the concentration field exhibit a clear dependency on the employed mesh type. Table 6 shows that particle concentration is increasing (in minimum, maximum and total values) with progressively more refined meshes. The clear convergence highlighted in Section 4.2 does not emerge in this case, due to the wall-adjacent cells being quite larger than the ones reached in the EVOL reactor sensitivity analysis.

Table 5
Computational mesh types employed for the MSFR case.

Mesh type	n° of cells	Base cell size (mm)	δ (mm)	Max aspect ratio
1	8.6×10^4	30	30	4.70
2	1.6×10^5	30	5.0	9.68
3	2.1×10^5	30	2.5	20.0
4	5.4×10^5	20	1.0	40.7
5	6.0×10^5	20	0.5	57.3
6	4.3×10^6	9	0.3	46.1

Table 6
Representative values of the 5Ms particle concentration in the MSFR simulations.

Mesh type	min C (part./m^3)	max C (part./m^3)	Tot Particles
1	1.90×10^{19}	5.81×10^{19}	5.46×10^{19}
2	2.12×10^{19}	4.68×10^{19}	4.51×10^{19}
3	2.47×10^{19}	4.94×10^{19}	4.84×10^{19}
4	4.33×10^{19}	7.18×10^{19}	7.33×10^{19}
5	1.11×10^{20}	1.36×10^{20}	1.44×10^{20}
6	2.62×10^{20}	2.90×10^{20}	3.16×10^{20}

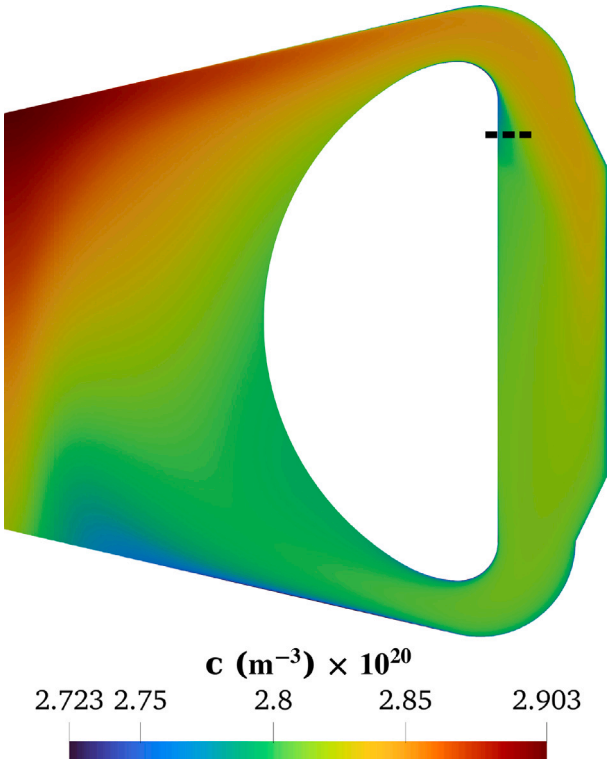

Fig. 11. 5Ms particles concentration field in the MSFR case. The dashed line indicates the sampling location.

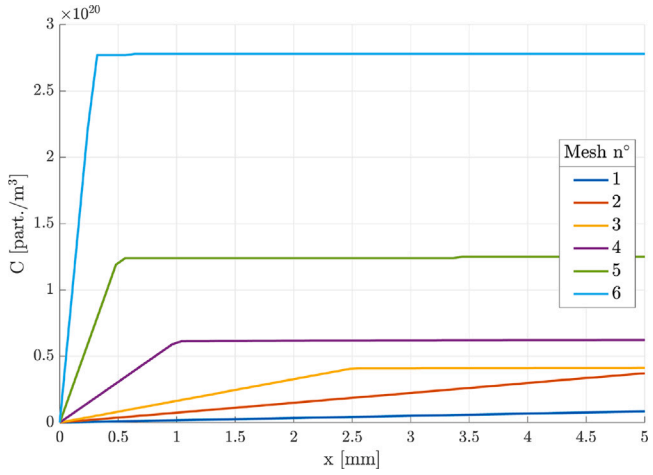

Fig. 12. Particle concentration profiles in the wall-normal direction from the point located $y = 0$ and $z = 0.7$ m.

Table 7
Total deposited 5Ms particles and surface concentration – at $y = 0$ and $z = 0.7$ m – in the MSFR simulation case, for the six mesh types. Total wall surface is 7.3 m^2.

Mesh type	Tot Deposited Particles	d (part./m^2)
1	2.530×10^{26}	1.07×10^{25}
2	2.533×10^{26}	5.23×10^{24}
3	2.530×10^{26}	9.62×10^{24}
4	2.532×10^{26}	1.28×10^{25}
5	2.531×10^{26}	6.60×10^{24}
6	2.452×10^{26}	4.00×10^{24}

Given the three-dimensional domain and relatively complex geometry and environment, comparing results cell-by-cell for each mesh type is not straightforward. Nevertheless, in order to gain insight on the deposition phenomena, the particle concentration field is sampled normally from the inner surface at an arbitrarily chosen location (see Fig. 11). Results of this sampling are shown in Fig. 12, where concentration profiles exhibit a clear dependence on the level of refinement.

Moving on to the deposition field, the total number of particles attached to the reactor walls shows no appreciable variation between mesh types, similarly to what emerged for the EVOL reactor (see Section 4.2). This might sound in contrast with the behavior seen previously for the total number of particles dispersed in the salt, considering that these two quantities are inversely correlated at equilibrium. It must be noted, however, that the total number of deposited particles is many orders of magnitude larger, so that the real trend is hidden within the numerical oscillations of different simulations. On the other hand, the value of the local deposition field is inversely proportional to the refinement level, as summarized in Table 7.

A more qualitative, yet complete picture of the impact on MSFR walls can be drawn from Fig. 13, in which the concentration of deposited particles is presented for the cooling circuit (i.e., the most affected region). First, it can be seen how the three most coarse mesh types produce fairly similar deposition patterns, with a slight progressive accumulation towards the hot spots. This is likely due to the field being closely related to the size of boundary cell faces, which in fact remains constant in cases 1 to 3, rather than the refinement profile itself. The maximum value of deposited particles, on the other hand, exhibit a stronger dependency. Such behavior is to be expected given that smaller wall-normal cell sizes are introduced with increasing

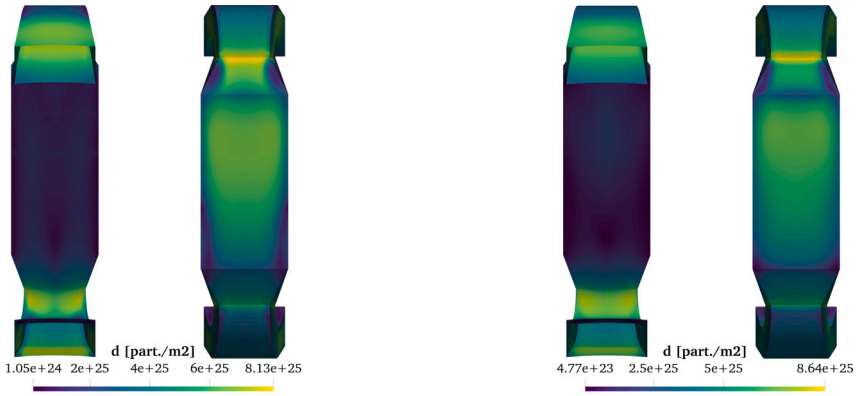

(a) Mesh type 1. (b) Mesh type 2.

(c) Mesh type 3. (d) Mesh type 4.

(e) Mesh type 5. (f) Mesh type 6.

Fig. 13. Calculated 5Ms particle deposition fields in the MSFR case. Front and back view of the cooling circuit.

refinement (see Table 5), hence achieving a better resolution of the particle concentration gradient.

A more evident correlation can be deduced by inspecting cases 4–6, in which the combination of smaller base cells and higher level of wall refinement produces a significant accumulation of particles in what is now a very thin hot spot. The distribution of deposited particles is inherently tied to the features of critical components such as the recirculation pump and heat exchanger, which in the present work have been modeled as simple volumes characterized by momentum source and heat sink, respectively.

In light of the presented results, the modeling of 5Ms particles seems to yield rather different – if not contradictory – outcomes when comparing MSFR and EVOL reactors. Albeit employing similar solver settings and thermophysical properties, the scenarios are dissimilar in terms of the environment being modeled. From reactor geometry, power and heat extraction, to the type of particles implemented. Nevertheless, the presented results confirm the strong correlation between deposition and mesh refinement. This fact, and the necessity of abating computational effort to perform more complex or transient analysis, prompted the implementation of the deposition boundary condition.

6.2. Deposition boundary condition

Taking into consideration the characteristics of the deposition phenomenon discussed previously, a tailored approach is proposed in this section to achieve satisfactory results with suboptimal mesh refinement.

Reprising the implementation of noble metals particles modeling presented in Section 3.1, the direct use of the boundary condition

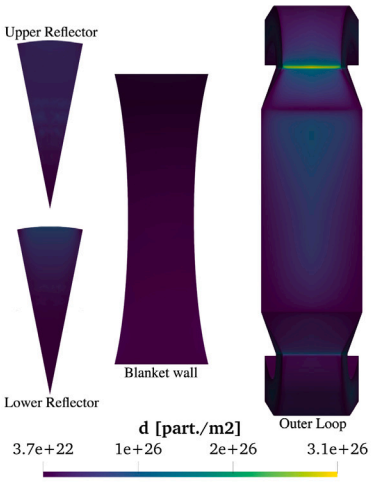

(a) Mesh case 6, employed to extract the deposition velocity γ.

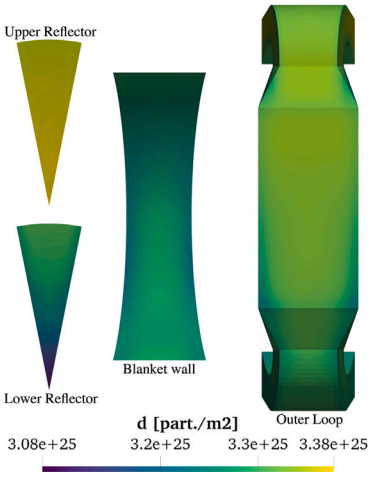

(b) Mesh case 1, obtained using a uniform value of $\gamma = 0.2$ mm/s for all surfaces.

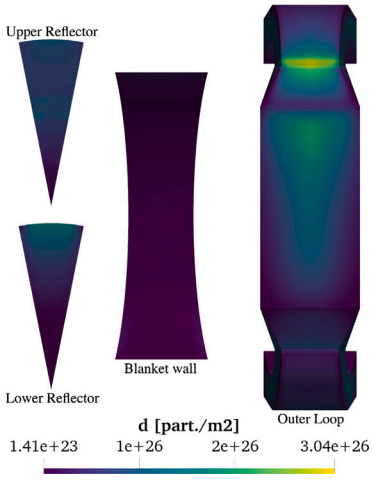

(c) Mesh case 1, obtained using the deposition velocity field as a whole.

Fig. 14. Particle deposition field for different cases concerning the proposed boundary condition for the MSFR 16th geometry.

requires some degree of knowledge on the deposition velocity γ. This need can be satisfied by the solution of the following equation:

$$\gamma = -D\frac{\nabla c \cdot \mathbf{n}}{c_{\text{avg}}} \tag{14}$$

where D is the particle mass diffusion coefficient, and $\nabla c \cdot \mathbf{n}$ and c_{avg} are the wall-normal gradient and average value of particle concentration respectively. To simplify the initial implementation stages, a single representative value was chosen, despite being an approximation of particle migration theory. However, the results obtained using the deposition velocity boundary condition, as discussed below, support the validity of this choice.

By running the MSFR case on mesh type 6, a reasonably accurate deposition field can be extracted through straightforward post-processing of the results (see (14)), without the need to solve additional iteration variables. Once this key quantity is obtained, two different approaches are tested. The first is to take the surface-averaged deposition velocity (roughly 0.2 mm/s assuming no particle removal) and plug it into the coarse mesh as a boundary condition. The intent is to find a single physically sound value for the MSFR specific environment, which can be used across different simulation scenarios to get a sense of the unfolding deposition phenomenon. Unfortunately, albeit foreseeable due to the rather diverse local conditions in the primary circuit, the results of this first strategy are definitely subpar. In fact, the model is not able to resolve the hot spot in the deposition field, yielding instead a rather uniform distribution, in addition to a misrepresentation of bulk particle concentration of about one order of magnitude.

Given these poor results, the second approach, which is the one finally proposed in this work, consists of employing the whole deposition velocity field extracted from the refined case as a face-by-face boundary condition for the coarse mesh. Fig. 14(c) shows a very good agreement between source and target simulations, both in terms of spatial distribution and local values. In particular, the deposition hot spot is resolved quite well, especially considering the large impact of numerical diffusion in mesh type 1 due to the size of boundary cell faces—6900 mm^2 against only 81 mm^2 of mesh type 6. The validity of the proposed method is further corroborated by the achieved reduction of computational resources. From around 1000 CPUh (Intel® Xeon® CPU E5-2630 v3 @ 2.40 GHz) required for mesh type 6 assuming

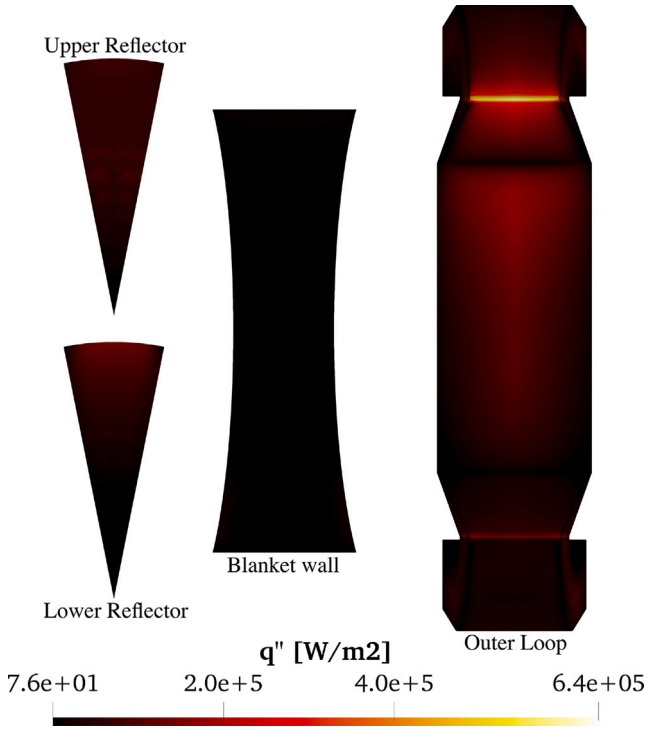

Fig. 15. Calculated decay heat flux field in the MSFR case.

perfectly absorbing walls, to less than 200 CPUh for mesh type 1 employing the custom boundary condition.

It is important to note that, although the results were obtained using the verified OpenFOAM solver, its application to the MSFR could not be validated due to the complete lack of suitable experimental data. One possible approach would have been to validate the code on a simpler geometry, potentially from a different application, where empirical data is available. However, no experimental setup was found that incorporates a combination of a distributed source term within the circulating fluid, a distributed sink term (e.g., radioactive decay), and deposition effects, which are key features of the MSR. While individual code subroutines could be validated using selected experimental datasets, this would provide only partial benefits, as the primary strength of the proposed framework lies in the coupled simulation of these phenomena. On the other hand, a powerful approach would be to validate the solver leveraging MSRE data, which, although limited in granularity, originates from careful measurements on the primary loop components. This would require applying the code not only to the reactor core but also to a simplified geometry of the primary loop to obtain deposition fields that are comparable with the available data (e.g. noble metals deposited on graphite, the primary heat exchanger, etc.). While this implementation would provide valuable insights, it was beyond the main scope of this work, and it is therefore left for future studies on the topic. As a conclusive remark, it should be taken into account the possibility of designing a dedicated experimental setup to validate the proposed model. This would ideally feature uranium salts circulating in a sub-critical loop, with the possibility of controlling the flow regime, and equipped with instrumentation capable of detecting decay radiation from deposited noble metals.

6.3. Decay heat from deposited particles

As anticipated in different MSRE-related studies (Kedl, 1972; Compere et al., 1975), a significant consequence of 5Ms deposition is the wall heat flux due to the radioactive decay of particles. Thanks to the model implementations proposed in this work, it is possible to take a first look at this phenomenon.

Fig. 15 gives a qualitative picture of the impact on primary circuit surfaces. It can be seen how the heat flux peaks at several hundreds kW/m^2 in the region of the hot spot, again assuming the absence of a particle removal system (bubbler). These values are not of significant concern during reactor operations, especially considering the limited hot spot surface area, and the 187 MW of fission power generated within the MSFR wedge used for the simulations. The same reasoning can be applied to the total decay heat released by deposited 5Ms particles in the primary circuit, which is only a little over 400 kW.

A somewhat different conclusion can be drawn when looking at the implications for transient scenarios, in particular during reactor shutdown after long periods of nominal operations. The localized decay heat can pose a serious threat to structural materials, hence requiring an adjustment in cooling power to avoid overheating. Even more so if a reactor core drainage is required at some point, since the deposited particle decay heat is not mitigated anymore by the primary salt flow. Considering these potential threats, reactor safety must be ensured through a dedicated cooling apparatus or, more effectively, a particle removal system that could avoid an excessive buildup of 5Ms particles.

7. Conclusions

In this paper, a tailored approach for modeling 5Ms particles in a typical MSFR environment has been presented. Building on the existing OpenFOAM multiphysics solver developed at Politecnico di Milano, key modifications were introduced, including the implementation of a deposition boundary condition and the adoption of a Pseudo-nuclide to embody the characteristics of all 5Ms nuclides present. This Eulerian single-phase framework was subsequently employed, with varying geometries and levels of detail, to investigate particle transport and deposition on reactor surfaces.

First, this model was verified against the analytical solution for a laminar flow in a horizontal channel with excellent agreement. A mesh sensitivity analysis was then performed employing a simplified reactor geometry and a generic particle. Simulations revealed that a strong correlation exists between mesh refinement and the quantities of interest. In particular, both bulk particle concentration and deposition vary noticeably, but eventually converge when reaching a sufficiently small wall-adjacent cell size (in the order of tens of microns).

The multiphysics code is then used to simulate a more realistic MSFR case scenario, with a more detailed reactor geometry and proper thermophysical and nuclear properties. Six mesh types featuring increasing refinement were generated to further investigate the correlation with noble metals particle fields. Due to a rapid explosion in computational requirements, even the most refined mesh was quite far from the wall-adjacent cell size reached in the sensitivity analysis. Nevertheless, compatible, and physically sound results were shown. In order to reduce the intensity of more complex, and possibly transient, simulations, this paper proposed to use the deposition velocity extracted in a highly-refined mesh as a boundary condition for coarse mesh simulations. By employing the whole deposition velocity field, it was possible to achieve satisfactory results with a 5x reduction in CPUh.

Finally, as a preliminary assessment, the additional heat due to noble metals particles decaying on the walls was presented. This highlighted a non-negligible impact on operations, especially during transient scenarios, further corroborating the need for a dedicated particle remover to ensure reactor safety.

CRediT authorship contribution statement

Nicolò Iaselli: Writing – review & editing, Writing – original draft, Software, Formal analysis, Conceptualization. **Antonio Cammi:** Supervision, Project administration. **Stefano Lorenzi:** Supervision, Project administration, Conceptualization.

Funding

This project has received funding from the Euratom research and training programme 2014–2018 under grant agreement No. 847527.

Disclaimer

The content of this paper does not reflect the official opinion of the European Union. Responsibility for the information and/or views expressed therein lies entirely with the authors.

Declaration of competing interest

The authors declare the following financial interests/personal relationships which may be considered as potential competing interests: Stefano Lorenzi reports financial support was provided by Euratom Research and Training Programme. If there are other authors, they declare that they have no known competing financial interests or personal relationships that could have appeared to influence the work reported in this paper.

Acknowledgments

A significant contribution to the realization of this work comes from Compute Canada (now Digital Research Alliance of Canada, DRAC), which provided valuable computational resources and effective technical support regarding OpenFOAM parallel computing.

Data availability

The data that support the findings of this study are openly available in Zenodo at http://doi.org/10.5281/zenodo.14017301.

References

Aufiero, M., Cammi, A., Geoffroy, O., Losa, M., Luzzi, L., Ricotti, M.E., Rouch, H., 2014. Development of an OpenFOAM model for the molten salt fast reactor transient analysis. Chem. Eng. Sci. 111, 390–401.

Benes, O., Konings, R., 2012. Molten Salt Reactor Fuel and Coolant. Elsevier, Amsterdam (The Netherlands), pp. 359–389.

Bittesnich, A., 2022. Analysis of the Source Term in Circulating Fuel Reactors: Burnup Results of the SAMOSAFER Benchmark. Politecnico di Milano, Milan, Italy.

Brenner, H., 1961. The slow motion of a sphere through a viscous fluid towards a plane surface. Chem. Eng. Sci. 16 (3), 242–251.

Brovchenko, M., Merle, E., 2013. Optimization of the pre-conceptual design of the MSFR - EVOL project. Deliverable D2.2 - EVOL project.

Caruggi, F., 2021. Multiphysics Modelling Approach for the Analysis of Xenon Removal Via Helium Bubbling in the Molten Salt Fast Reactor. Politecnico di Milano, Milan, Italy.

Cervi, E., Lorenzi, S., Cammi, A., Luzzi, L., 2019. Development of a multiphysics model for the study of fuel compressibility effects in the molten salt fast reactor. Chem. Eng. Sci. 193, 379–393.

Chourdakis, G., Schneider, D., Uekermann, B., 2023. OpenFOAM-preCICE: Coupling OpenFOAM with external solvers for multi-physics simulations. OpenFOAM® J. 3, 1–25.

Compere, E.L., Kirslis, S.S., Bohlmann, E.G., Blankenship, F.F., Grimes, W.R., 1975. Fission Product Behavior in the Molten Salt Reactor Experiment (ORNL-4865). Oak Ridge National Lab. (ORNL), Oak Ridge, TN (United States.

Delpech, S., Merle-Lucotte, E., Heuer, D., Allibert, M., Ghetta, V., Le-Brun, C., Doligez, X., Picard, G., 2009. Reactor physic and reprocessing scheme for innovative molten salt reactor system. J. Fluor. Chem. 130 (1), 11–17.

Di Ronco, A., Lorenzi, S., Giacobbo, F., Cammi, A., 2021. An Eulerian single-phase transport model for solid fission products in the molten salt fast reactor: Development of an analytical solution for verification purposes. Front. Energy Res. 9.

Di Ronco, A., Lorenzi, S., Giacobbo, F., Cammi, A., 2022. Multiphysics analysis of RANS-based turbulent transport of solid fission products in the molten salt fast reactor. Nucl. Eng. Des. 391.

Fiorina, C., Kerkar, N., Mikityuk, K., Rubiolo, P., Pautz, A., 2016. Development and verification of the neutron diffusion solver for the GeN-foam multi-physics platform. Ann. Nucl. Energy 96, 212–222.

Fiorina, C., Lathouwers, D., Aufiero, M., Cammi, A., Guerrieri, C., Kloosterman, J.L., Luzzi, L., Ricotti, M.E., 2014. Modelling and analysis of the MSFR transient behaviour. Ann. Nucl. Energy 64, 485–498.

Frederix, E., Kuczaj, A., Nordlund, M., Veldman, A., Geurts, B., 2017. Eulerian modeling of inertial and diffusional aerosol deposition in bent pipes. Comput. & Fluids 159, 217–231.

Gladinez, K., Rosseel, K., Lim, J., Marino, A., Heynderickx, G., Aerts, A., 2019. Formation and transport of lead oxide in a non-isothermal lead-bismuth eutectic loop. Nucl. Eng. Des. 349, 78–85.

Hébert, A., 2010. Multigroup neutron transport and diffusion computations. Handb. Nucl. Eng. 751–911.

Jasak, H., 2009. OpenFOAM: Open source CFD in research and industry. Int. J. Nav. Archit. Ocean. Eng. 1 (2), 89–94.

Kedl, R.J., 1972. Migration of a Class of Fission Products (Noble Metals) in the Molten-Salt Reactor Experiment (ORNL-3884). Technical Report, Oak Ridge National Lab. (ORNL), Oak Ridge, TN (United States.

Krause, F., Wenk, A., Lacor, C., Kreyling, W.G., Möller, W., Verbanck, S., 2013. Numerical and experimental study on the deposition of nanoparticles in an extrathoracic oral airway model. J. Aerosol Sci. 57, 131–143.

Launder, B., Spalding, D., 1974. The numerical computation of turbulent flows. Comput. Methods Appl. Mech. Engrg. 3, 269–289.

Liu, B.Y., Agarwal, J.K., 1974. Experimental observation of aerosol deposition in turbulent flow. J. Aerosol Sci. 5 (2), 145–155.

Marino, A., Peltomäki, M., Lim, J., Aerts, A., 2020. A multi-physics computational tool based on CFD and GEM chemical equilibrium solver for modeling coolant chemistry in nuclear reactors. Prog. Nucl. Energy 120, 103190.

Patankar, S.V., Spalding, D.B., 1972. A calculation procedure for heat, mass and momentum transfer in three-dimensional parabolic flows. Int. J. Heat Mass Transfer IS, 1787–1806.

Price, T., Chvala, O., Bereznai, G., 2020. A dynamic model of xenon behavior in the molten salt reactor experiment. Ann. Nucl. Energy 144, 107535.

Prieve, D.C., Ruckenstein, E., 1976. Rates of deposition of brownian particles calculated by lumping interaction forces into a boundary condition. J. Colloid Interface Sci. 57 (3), 547–550.

Ruckenstein, E., Prieve, D.C., 1973. Rate of deposition of Brownian particles under the action of London and double-layer forces. J. Chem. Soc., Faraday Trans. 2 69, 1522–1536.

Scuro, N., Beneš, O., Lorenzi, S., Krstovic, M., Krepel, J., Piro, M., 2024. Coupled computational fluid dynamics and computational thermodynamics simulations for fission product retention and release: A molten salt fast reactor application. Prog. Nucl. Energy 177, 105450.

Stempniewicz, M., Roelofs, F., 2021. Molten salt modelling in spectra applied to MSRE. Nucl. Eng. Des. 384, 111483.

Walker, S.A., Ji, W., 2021. Species transport analysis of noble metal fission product transport, deposition, and extraction in the molten salt reactor experiment. Ann. Nucl. Energy 158, 108250.